PERGAMON

International Journal of Solids and Structures 37 (2000) 5097–5122

INTERNATIONAL JOURNAL OF SOLIDS and STRUCTURES

www.elsevier.com/locate/ijsolstr

A strain-compatible method for micromechanical analysis of multi-phase composites

Hewen Gan, Carlos E. Orozco*, Carl T. Herakovich

Department of Civil Engineering, University of Virginia, Charlottesville, VA 22903, USA

Received 23 November 1998; in revised form 14 July 1999

Abstract

A new method for micromechanical analysis of multi-phase composites is presented. The new method is inspired by the generalized method of cells which is widely utilized in the field of composite mechanics. The new method, called strain-compatible method of cells, exhibits the so called shear coupling effect, absent in the generalized method of cells. Because of this shear coupling, the method is especially useful when shear effects are important. In the present study, the new method is used to predict the micro-stresses and to model the effective elastic constants of unidirectional composites. Results obtained with the strain-compatible method of cells compare very well with those of well-established traditional tools like finite element analysis. A variety of numerical results comparing the accuracy and performance of the new method with those of the generalized method of cells, the finite element method, and the classical Reuss and Voigt approximations is presented.

Keywords: Composite mechanics; Micromechanical models

1. Introduction

The objective of micromechanical models of composites is to predict the effective (or macro or average) properties and behavior of the composite starting from the properties and behavior of its constituents. The simplest and oldest micromechanical models are those due to Voigt (1889) and Reuss (1929). These are called the ''Voigt Approximation'', and the ''Reuss Approximation'', respectively. More recently, many other micromechanical models have been proposed, e.g., the Concentric Cylinder Assembly Model (CCA) (Hashin and Rosen, 1964), the Self-Consistent Method (Hill, 1965; Budiansky,

* Corresponding author. Fax: +1-804-982-2951.
E-mail address: ceo7f@virginia.edu (C.E. Orozco).

0020-7683/00/$ - see front matter
PII: S0020-7683(99)00199-7

1965), the Mori–Tanaka Method (Mori and Tanaka, 1973), and the Generalized Method of Cells (GMC) (Paley and Aboudi, 1992; Aboudi, 1996). Some of these methods are known to give erroneous results in some limiting situations. The Reuss approximation for instance produces incorrect results for the fiber-direction Young's modulus, while the Voigt approximation produces its greatest error when estimating the transverse shear modulus. This of course is a consequence of the fact that the Voigt and Reuss approximations represent upper and lower bounds for the stiffness matrix coefficients of a given composite (e.g., see Herakovich, 1998). On the other hand, the more refined models also have their shortcomings. The Mori–Tanaka method for instance, produces erroneous results in some limiting cases (Benveniste, 1987). And the generalized method of cells (GMC) exhibits a lack of what can be termed *shear coupling*. Shear coupling refers to the fact that the transverse shear stresses on a composite are in general nonzero when the composite is subjected to a transverse normal stress. It is well known however that GMC approximates these stresses as zero. The development of the strain-compatible method of cells (SCMC) was motivated by the desire to remedy this lack of shear coupling.

Both GMC and SCMC are volume-averaging, micromechanical analysis tools that provide accurate estimates of the effective mechanical properties and average responses of composites given the properties and behavior of the constituents. One of the advantages of volume-averaging methods over standard numerical analysis tools like the finite element method (FEM), is that they provide a 3D characterization of the composite given a 2D discretization of its cross-section. The discretization process in volume-averaging methods involves the identification of so called representative volume elements (RVEs) or unit cells which are subsequently divided into subcells.

When a particular set of assumptions or requirements regarding averaging of stresses and strains, continuity of stresses and strains, and/or compatibility of strains is adopted, a specific method is obtained. The generalized method of cells for instance requires displacement and traction continuity among cells and subcells. In contrast, the new strain-compatible method of cells requires equilibrium of cells and subcells and compatibility of strains. As a consequence of the latter requirements, SCMC exhibits the desired shear coupling between normal and shear stresses. Furthermore, SCMC predictions are very close to those of the finite element method.

In the following sections, the fundamentals of GMC and the new SCMC are presented. This is followed by a series of numerical results for the problems of finding the effective elastic constants and the distribution of micro-stresses in unidirectional composites.

2. Volume-averaging methods

Volume-averaging methods for micromechanical analysis of multi-phase composites rely on the idea that it should be possible to obtain approximate expressions for the effective properties and behavior of the composite by volume-averaging either the material properties, or the stresses and strains in the constituents. In particular, GMC and SCMC are both volume-averaging methods in which the effective properties and behavior are obtained by volume-averaging the stresses and strains in the composite.

When applied to unidirectional composites, both GMC and SCMC start from a discretized two-dimensional representation of a typical cross-section of the composite. A portion of this cross-section is identified as a *representative* volume element (RVE). Fig. 1 depicts one such RVE. It is assumed that the fibers of this unidirectional composite are directed in the x_1 direction. The RVE should be large enough to capture the essence of the composite properties and behavior, yet small enough to minimize the computational burden[1]. For the purposes of the present discussion, it is going to be assumed that a

[1] For details about how to choose the size of an RVE see e.g., (Ostoja-Starzewski, 1998).

proper RVE has been chosen. The RVE is assumed to repeat itself in the x_2 and x_3 directions. In the context of GMC and SCMC, the RVE is also identified with a so called unit cell. Each unit cell is divided into $N_\beta N_\gamma$ subcells, each of which can have different material properties (Fig. 1).

Both GMC and SCMC can be thought of as based on the following fundamental assumption:

Each RVE can be mapped into a single point belonging to a homogeneous deformation field with displacement $\mathbf{w}$ *and displacement gradient* $\nabla\mathbf{w}$.

In addition to this fundamental assumption, GMC and SCMC share the following specific assumptions:

Common GMC and SCMC Specific Assumptions:

1. The displacements are continuous along cell and subcell interfaces and the strains are constant within the subcells.
2. The unit cell stresses and strains are periodic (the RVE repeats itself in the x_2 and x_3 directions, so it repeats itself with all its attributes).

There are also specific assumptions to GMC and SCMC. These are:

Specific GMC Assumption:

3. There is traction continuity across all cell and subcell interfaces.

Specific SCMC Assumptions:

3. Subcell stresses satisfy the equilibrium equations.
4. Subcell strains satisfy the Saint–Venant's compatibility conditions.

2.1. Average strain relationships

The fundamental assumption and the specific assumptions 1 and 2 above (shared by both GMC and SCMC) can be explicitly stated in terms of strains. To this end, the displacement gradient $\nabla\mathbf{w}$ is chosen such that the components of the small strain tensor correspond exactly to the average (or effective) strains. That is, the components of $\mathbf{E} \equiv \frac{1}{2}(\nabla^{\mathrm{T}}\mathbf{w} + \nabla\mathbf{w})$ are the following:

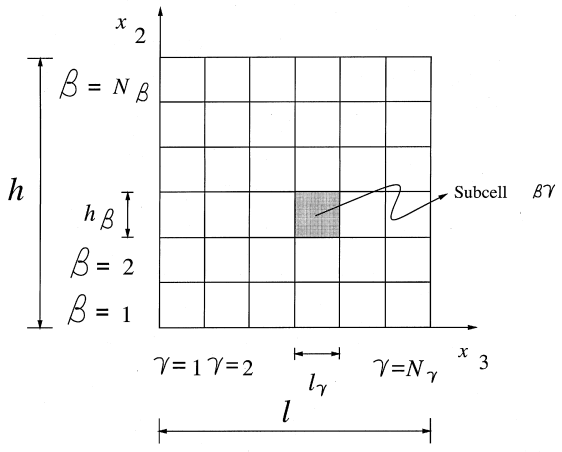

Fig. 1. Repeating unit cell (or RVE) with subcells and nomenclature.

$$\bar{\varepsilon}_{11} = \varepsilon_{11}^{\beta\gamma}, \quad \forall\, \beta, \gamma \tag{1}$$

$$\bar{\varepsilon}_{22} = \frac{1}{h}\sum_{\beta}^{N_\beta} \varepsilon_{22}^{(\beta\gamma)} h_\beta, \quad \gamma = 1, N_\gamma \tag{2}$$

$$\bar{\varepsilon}_{12} = \frac{1}{h}\sum_{\beta}^{N_\beta} \varepsilon_{12}^{(\beta\gamma)} h_\beta, \quad \gamma = 1, N_\gamma \tag{3}$$

$$\bar{\varepsilon}_{33} = \frac{1}{l}\sum_{\gamma}^{N_\gamma} \varepsilon_{33}^{(\beta\gamma)} l_\gamma, \quad \beta = 1, N_\beta \tag{4}$$

$$\bar{\varepsilon}_{13} = \frac{1}{l}\sum_{\gamma}^{N_\gamma} \varepsilon_{13}^{(\beta\gamma)} l_\gamma, \quad \beta = 1, N_\beta \tag{5}$$

and,

$$\bar{\varepsilon}_{23} = \frac{1}{hl}\sum_{\beta}^{N_\beta}\sum_{\gamma}^{N_\gamma} \varepsilon_{23}^{(\beta\gamma)} h_\beta l_\gamma \tag{6}$$

Note that with the exception of Eq. (1), these equations represent averages that are particular instances of the general expression for effective average strain:

$$\bar{\varepsilon}_{ij} \equiv \frac{1}{hl}\sum_{\gamma}^{N_\gamma}\sum_{\beta}^{N_\beta} h_\beta l_\gamma \varepsilon_{ij}^{(\beta\gamma)} \tag{7}$$

Note that the averages corresponding to $\bar{\varepsilon}_{22}$ and $\bar{\varepsilon}_{12}$ are carried out with respect to the β direction only, while the averages corresponding to $\bar{\varepsilon}_{33}$ and $\bar{\varepsilon}_{13}$ are carried out with respect to the γ direction only. This is necessary to guarantee the continuity of displacements across RVE interfaces.

Eqs. (1)–(6) can be written in matrix form as:

$$\mathbf{A}_G \varepsilon_s = \mathbf{J}\bar{\varepsilon} \tag{8}$$

where $\varepsilon_s \equiv \{\varepsilon^{(1,\,1)}, \varepsilon^{(1,\,2)}, \ldots, \varepsilon^{(N_\beta,\,N_\gamma)}\}^{\mathrm{T}}$ contains $N_\beta N_\gamma$ vectors with the subcell strains, and $\bar{\varepsilon} \equiv \{\bar{\varepsilon}_{11}, \bar{\varepsilon}_{22}, \bar{\varepsilon}_{33}, 2\bar{\varepsilon}_{23}, 2\bar{\varepsilon}_{13}, 2\bar{\varepsilon}_{12}\}^{\mathrm{T}}$ contains the effective strains. The matrices $\mathbf{A}_G$ and $\mathbf{J}$ in (7) contain information about the subcell and cell geometry. Their entries are h_β's, l_γ's, $h_\beta l_\gamma$ products; h's, l's, hl products; and ones and zeros.

3. The generalized method of cells

As mentioned, GMC and SCMC differ in assumptions 3 and 4. In the following section, the equations corresponding to GMC's specific assumption 3, i.e., traction continuity, are presented.

3.1. Traction continuity conditions (GMC)

Assuming that the effective strains $\bar{\varepsilon}$ are specified, Eq. (8) can be regarded as a system of $2(N_\beta + N_\gamma) + N_\beta N_\gamma + 1$ equations containing $6N_\beta N_\gamma$ unknown subcell strains. In the context of GMC, the remaining $5N_\beta N_\gamma - 2(N_\beta + N_\gamma) - 1$ equations needed to find the complete set of subcell strains are provided by traction continuity conditions at the subcell interfaces (Paley and Aboudi, 1992). These traction continuity conditions are the following (see Fig. 1):

$$\sigma_{22}^{(\beta\gamma)} = \sigma_{22}^{(\beta+1,\,\gamma)}, \quad \beta = 1, N_\beta - 1, \gamma = 1, N_\gamma \tag{9}$$

$$\sigma_{33}^{(\beta\gamma)} = \sigma_{33}^{(\beta,\,\gamma+1)}, \quad \beta = 1, N_\beta, \gamma = 1, N_\gamma - 1 \tag{10}$$

$$\sigma_{23}^{(\beta\gamma)} = \sigma_{23}^{(\beta+1,\,\gamma)}, \quad \beta = 1, N_\beta - 1, \gamma = 1, N_\gamma \tag{11}$$

$$\sigma_{32}^{(\beta\gamma)} = \sigma_{32}^{(\beta,\,\gamma+1)}, \quad \beta = N_\beta, \gamma = 1, N_\gamma - 1 \tag{12}$$

$$\sigma_{21}^{(\beta\gamma)} = \sigma_{21}^{(\beta+1,\,\gamma)}, \quad \beta = 1, N_\beta - 1, \gamma = 1, N_\gamma \tag{13}$$

$$\sigma_{31}^{(\beta\gamma)} = \sigma_{31}^{(\beta,\,\gamma+1)}, \quad \beta = 1, N_\beta, \gamma = 1, N_\gamma - 1 \tag{14}$$

The foregoing traction continuity conditions can be written in terms of subcell strains as:

$$\mathbf{A}_M \boldsymbol{\varepsilon}_s = \mathbf{0} \tag{15}$$

if use is made of the elasticity constitutive relationships:

$$\boldsymbol{\sigma}^{(\beta\gamma)} = \mathbf{C}^{(\beta\gamma)} \boldsymbol{\varepsilon}^{(\beta\gamma)} \tag{16}$$

In Eq. (16), $\mathbf{C}^{(\beta\gamma)}$ represents the elastic stiffness matrix of subcell (β, γ), and $\boldsymbol{\varepsilon}^{(\beta\gamma)} \equiv \{\varepsilon_{11}^{(\beta\gamma)}, \varepsilon_{22}^{(\beta\gamma)}, \varepsilon_{33}^{(\beta\gamma)}, 2\varepsilon_{23}^{(\beta\gamma)}, 2\varepsilon_{13}^{(\beta\gamma)}, 2\varepsilon_{12}^{(\beta\gamma)}\}^{\mathrm{T}}$ is a vector of the subcell strains. The matrix $\mathbf{A}_M$ is then a $5N_\beta N_\gamma - 2(N_\beta + N_\gamma) - 1 \times 6N_\beta N_\gamma$ matrix that contains entries of the individual elastic stiffness matrices of all subcells.

Eqs. (8) and (15) can be combined into a single equation as follows:

$$\mathbf{A}\boldsymbol{\varepsilon}_s = \mathbf{K}\bar{\boldsymbol{\varepsilon}} \tag{17}$$

where,

$$\mathbf{A} \equiv \begin{bmatrix} \mathbf{A}_G \\ \mathbf{A}_M \end{bmatrix} \tag{18}$$

and,

$$\mathbf{K} \equiv \begin{bmatrix} \mathbf{J} \\ \mathbf{0} \end{bmatrix} \tag{19}$$

Eq. (17) constitutes a system of $6N_\beta N_\gamma$ equations with $6N_\beta N_\gamma$ unknowns (assuming the effective average strains are known). The solution of this system of equations constitutes the core of the computations for GMC.

4. The strain-compatible method of cells

The fundamental assumption, as well as the specific assumptions 1 and 2 above are invoked by SCMC and GMC. However, instead of traction continuity, SCMC assumes equilibrium of cells and subcells and compatibility of strains.

It should be emphasized that under the assumption of constant subcell strains, GMC's traction continuity assumption amounts to an automatic satisfaction of the (discretized) equilibrium equations. However, the reciprocal is not true, i.e., satisfaction of equilibrium does not necessarily imply traction continuity across cell and subcell interfaces. In this sense, SCMC can be regarded as a method in which GMC's assumption of traction continuity is relaxed to simply require equilibrium of cells and subcells. Furthermore, the assumption of continuity of displacements across cell and subcell interfaces (assumption 1 above) does not necessarily guarantee a unique displacement field. In order to guarantee a unique displacement field, SCMC assumptions 1, 2 and 3 must be supplemented with the Saint–Venant's compatibility conditions (assumption 4 above).

4.1. Equilibrium equations (SCMC)

For a unidirectional composite with the fibers in the x_1 direction and an x_1-independent loading, the equilibrium equations of elasticity reduce to:

$$\frac{\partial \sigma_{12}}{\partial x_2} + \frac{\partial \sigma_{13}}{\partial x_3} = 0 \tag{20}$$

$$\frac{\partial \sigma_{22}}{\partial x_2} + \frac{\partial \sigma_{23}}{\partial x_3} = 0 \tag{21}$$

$$\frac{\partial \sigma_{32}}{\partial x_2} + \frac{\partial \sigma_{33}}{\partial x_3} = 0 \tag{22}$$

Discrete forms of these equations are presented in Section 4.3 below.

4.2. Compatibility relationships (SCMC)

A salient feature of SCMC is that it enforces Saint–Venant's strain compatibility conditions. This is done in an approximate fashion by means of finite differences. The process is as follows:

Saint–Venant's compatibility equations are:

$$\frac{\partial^2 \varepsilon_{11}}{\partial x_2^2} + \frac{\partial^2 \varepsilon_{22}}{\partial x_1^2} - \frac{2\partial^2 \varepsilon_{12}}{\partial x_1 \partial x_2} = 0 \tag{23}$$

$$\frac{\partial^2 \varepsilon_{22}}{\partial x_3^2} + \frac{\partial^2 \varepsilon_{33}}{\partial x_2^2} - 2\frac{\partial^2 \varepsilon_{23}}{\partial x_2 \partial x_3} = 0 \tag{24}$$

$$\frac{\partial^2 \varepsilon_{33}}{\partial x_1^2} + \frac{\partial^2 \varepsilon_{11}}{\partial x_3^2} - 2\frac{\partial^2 \varepsilon_{13}}{\partial x_1 \partial x_3} = 0 \tag{25}$$

$$-\frac{\partial^2 \varepsilon_{11}}{\partial x_2 \partial x_3} + \frac{\partial}{\partial x_1}\left(-\frac{\partial \varepsilon_{23}}{\partial x_1} + \frac{\partial \varepsilon_{31}}{\partial x_2} + \frac{\partial \varepsilon_{12}}{\partial x_3}\right) = 0 \tag{26}$$

$$-\frac{\partial^2 \varepsilon_{22}}{\partial x_1 \partial x_3} + \frac{\partial}{\partial x_2}\left(-\frac{\partial \varepsilon_{31}}{\partial x_2} + \frac{\partial \varepsilon_{12}}{\partial x_3} + \frac{\partial \varepsilon_{23}}{\partial x_1}\right) = 0 \tag{27}$$

$$-\frac{\partial^2 \varepsilon_{33}}{\partial x_1 \partial x_2} + \frac{\partial}{\partial x_3}\left(-\frac{\partial \varepsilon_{12}}{\partial x_3} + \frac{\partial \varepsilon_{23}}{\partial x_1} + \frac{\partial \varepsilon_{31}}{\partial x_2}\right) = 0 \tag{28}$$

As a consequence of the unidirectionality of the composite, all derivatives involving x_1 in (23)–(28) are equal to zero. Also, from Eq. (1) all derivatives involving ε_{11} are zero. As a result, Eqs. (23), (25) and (26) are satisfied identically. And Eqs. (27) and (28) reduce to the simpler forms:

$$\frac{\partial}{\partial x_2}\left(-\frac{\partial \varepsilon_{31}}{\partial x_2} + \frac{\partial \varepsilon_{12}}{\partial x_3}\right) = 0 \tag{29}$$

$$\frac{\partial}{\partial x_3}\left(-\frac{\partial \varepsilon_{12}}{\partial x_3} + \frac{\partial \varepsilon_{31}}{\partial x_2}\right) = 0 \tag{30}$$

Integrating Eq. (29) with respect to x_2 and Eq. (30) with respect to x_3, we obtain:

$$-\frac{\partial \varepsilon_{31}}{\partial x_2} + \frac{\partial \varepsilon_{12}}{\partial x_3} = C_2(x_3)$$

and,

$$-\frac{\partial \varepsilon_{31}}{\partial x_2} + \frac{\partial \varepsilon_{12}}{\partial x_3} = C_3(x_2)$$

or,

$$\frac{\partial \varepsilon_{12}}{\partial x_3} - \frac{\partial \varepsilon_{13}}{\partial x_2} = \text{constant} = C \tag{31}$$

In order to evaluate the constant in Eq. (31), we integrate this equation over the RVE, to obtain,

$$Chl = \int_0^h \int_0^l \left(\frac{\partial \varepsilon_{12}}{\partial x_3} - \frac{\partial \varepsilon_{13}}{\partial x_2}\right) \mathrm{d}x_3 \, \mathrm{d}x_2$$

or,

$$Chl = \int_0^h \left(\int_0^l \frac{\partial \varepsilon_{12}}{\partial x_3} \, \mathrm{d}x_3 \right) \mathrm{d}x_2 - \int_0^l \left(\int_0^h \frac{\partial \varepsilon_{13}}{\partial x_2} \, \mathrm{d}x_2 \right) \mathrm{d}x_3$$

or,

$$Chl = \int_0^h \left[\varepsilon_{12}(x_2, l) - \varepsilon_{12}(x_2, 0) \right] \mathrm{d}x_2 - \int_0^l \left[\varepsilon_{13}(h, x_3) - \varepsilon_{13}(0, x_3) \right] \mathrm{d}x_3$$

which yields,

$$Chl = 0$$

when the periodicity of strains is invoked. Therefore, the constant in Eq. (31) is zero and the equation becomes:

$$\frac{\partial \varepsilon_{12}}{\partial x_3} - \frac{\partial \varepsilon_{13}}{\partial x_2} = 0 \tag{32}$$

We are then left with Eqs. (24) and (32) from the strain compatibility conditions. Discrete versions of these equations are presented below.

4.3. Equilibrium and compatibility equations: discrete form

The average strain relationships summarized in Eqs. (1)–(6) are already in discrete form. The additional equilibrium and compatibility equations required by SCMC must be discretized to allow for a numerical solution. We use a combination of forward, backward, and central finite differences for this purpose. Sample discrete equations resulting from the application of finite differences to the equilibrium and compatibility equations are given next.

4.3.1. Explicit equilibrium equations

Eqs. (20)–(22) are approximated by forward and backward differences. Referring for instance to subcell (1, 1) in Fig. 2, Eq. (21) takes the form:

$$\frac{\sigma_{22}^{(2,1)} - \sigma_{22}^{(1,1)}}{0.5(h_1 + h_2)} + \frac{\sigma_{23}^{(1,1)} - \sigma_{23}^{(3,1)}}{0.5(l_1 + l_2)} = 0 \tag{33}$$

Since there are $N_\beta N_\gamma$ subcells per RVE (Fig. 1), there should be $N_\beta N_\gamma$ discrete equations for each of Eqs. (20)–(22). However, due to the periodicity of the stresses, only $N_\beta N_\gamma - 1$ equations corresponding

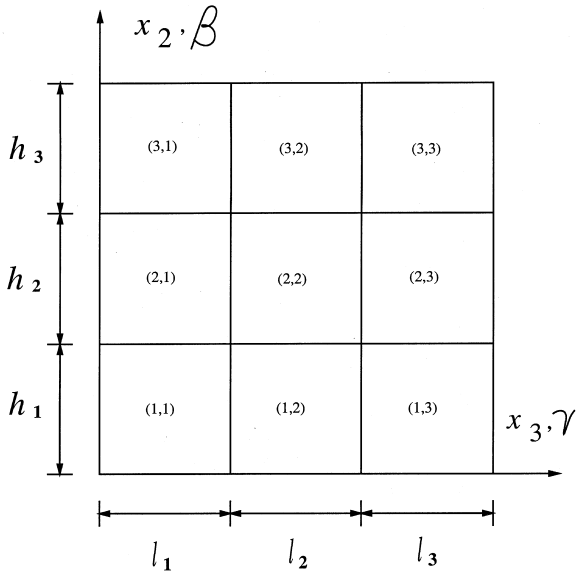

Fig. 2. 3 × 3 unit cell to illustrate finite difference procedure.

to each of these equations are independent. This is shown by integrating Eqs. (20)–(22) over the entire RVE as follows. Taking Eq. (20) for instance, we obtain:

$$\int_0^h \int_0^l \left(\frac{\partial \sigma_{12}}{\partial x_2} + \frac{\partial \sigma_{13}}{\partial x_3} \right) \mathrm{d}x_3 \, \mathrm{d}x_2 = \int_0^l \left(\int_0^h \frac{\partial \sigma_{12}}{\partial x_2} \, \mathrm{d}x_2 \right) \mathrm{d}x_3 + \int_0^h \left(\int_0^l \frac{\partial \sigma_{13}}{\partial x_3} \, \mathrm{d}x_3 \right) \mathrm{d}x_2$$

or,

$$\int_0^h \int_0^l \left(\frac{\partial \sigma_{12}}{\partial x_2} + \frac{\partial \sigma_{13}}{\partial x_3} \right) \mathrm{d}x_3 \, \mathrm{d}x_2 = \int_0^l \left[\sigma_{12}(h, x_3) - \sigma_{12}(0, x_3) \right] \mathrm{d}x_3 + \int_0^h \left[\sigma_{13}(x_2, l) - \sigma_{13}(x_2, 0) \right] \mathrm{d}x_2$$

Invoking the periodicity of stresses this yields,

$$\int_0^h \int_0^l \left(\frac{\partial \sigma_{12}}{\partial x_2} + \frac{\partial \sigma_{13}}{\partial x_3} \right) \mathrm{d}x_3 \, \mathrm{d}x_2 \equiv 0 \tag{34}$$

Similarly, from Eq. (21), we obtain,

$$\int_0^h \int_0^l \left(\frac{\partial \sigma_{22}}{\partial x_2} + \frac{\partial \sigma_{23}}{\partial x_3} \right) \mathrm{d}x_3 \, \mathrm{d}x_2 \equiv 0 \tag{35}$$

and from Eq. (22),

$$\int_0^h \int_0^l \left(\frac{\partial \sigma_{32}}{\partial x_2} + \frac{\partial \sigma_{33}}{\partial x_3} \right) \mathrm{d}x_3 \, \mathrm{d}x_2 \equiv 0 \tag{36}$$

It is evident that the integration of each of Eqs. (20)–(22) over the RVE should yield zero. However, Eqs. (34)–(36) show that, due to the periodicity of stresses, each of these equations is satisfied as an identity. Since each of Eqs. (34)–(36) is the continuous version of the sum of discrete equations like Eq. (33) for all subcells, it follows that the sum of discrete equations like Eq. (33) for all subcells is equal to zero. Therefore, all but one of the discrete equilibrium equations corresponding to each of Eqs. (20)–(22) are independent. That is, only $N_\beta N_\gamma - 1$ of the $N_\beta N_\gamma$ equations for each of (20)–(22) are independent. We then have a total of $3(N_\beta N_\gamma - 1)$ independent equations from equilibrium. These equations can be expressed in terms of strains by means of appropriate constitutive relationships.

4.3.2. Explicit compatibility equations

Saint–Venant's strain compatibility equations are approximated by means of forward and central finite differences. Referring to subcell (2, 2) in Fig. 2, the first term of Eq. (24) is approximated as:

$$\frac{\partial^2 \varepsilon_{22}}{\partial x_3^2} \approx \frac{\varepsilon_{22}^{(2,3)} - \varepsilon_{22}^{(2,2)}}{0.25 l_2 (l_2 + l_3) + 0.125 (l_1 + l_3)(l_2 + l_3)} - \frac{\varepsilon_{22}^{(2,2)} - \varepsilon_{22}^{(2,1)}}{0.25 l_2 (l_1 + l_2) + 0.125 (l_1 + l_3)(l_1 + l_2)} \tag{37}$$

The other two terms in Eq. (24) give rise to similar expressions. The remaining compatibility equation (Eq. (32)) results in an approximation analogous to that of Eq. (33).

Since there are $N_\beta N_\gamma$ subcells, there should be $N_\beta N_\gamma$ discrete equations corresponding to each of Eqs. (24) and (32). Due to the periodicity of the strains however, not all of these $N_\beta N_\gamma$ equations are independent. In fact, only $(N_\beta - 1)(N_\gamma - 1)$ of the $N_\beta N_\gamma$ equations corresponding to each of Eqs. (24) and (32) are independent. The reasoning is analogous to that used for the discrete equilibrium equations in the previous section. Taking for instance Eq. (32), we proceed as follows:

Integrating Eq. (32) in the x_2 direction yields:

$$\int_0^h \left(\frac{\partial \varepsilon_{12}}{\partial x_3} - \frac{\partial \varepsilon_{13}}{\partial x_2} \right) \mathrm{d}x_2 = -\left[\varepsilon_{13}(h, x_3) - \varepsilon_{13}(0, x_3) \right] + \frac{\partial}{\partial x_3} \int_0^h \varepsilon_{12} \, \mathrm{d}x_2$$

Invoking the periodicity of strains, this becomes,

$$\int_0^h \left(\frac{\partial \varepsilon_{12}}{\partial x_3} - \frac{\partial \varepsilon_{13}}{\partial x_2} \right) \mathrm{d}x_2 = 0 + \frac{\partial}{\partial x_3} [h \bar{\varepsilon}_{12}]$$

or,

$$\int_0^h \left(\frac{\partial \varepsilon_{12}}{\partial x_3} - \frac{\partial \varepsilon_{13}}{\partial x_2} \right) \mathrm{d}x_2 \equiv 0$$

Analogously, integrating Eq. (32) in the x_3 direction, gives,

$$\int_0^l \left(\frac{\partial \varepsilon_{12}}{\partial x_3} - \frac{\partial \varepsilon_{13}}{\partial x_2} \right) \mathrm{d}x_3 \equiv 0$$

A pair of similar identities is obtained for Eq. (24). Since these integrals are continuous versions of the sums of the discrete versions of Eqs. (24) and (32) in the β and γ directions, it follows that the sums of the discrete versions of Eqs. (24) and (32) in the β and γ directions are equal to zero. Therefore, only $(N_\beta - 1)(N_\gamma - 1)$ of the $N_\beta N_\gamma$ equations corresponding to each of Eqs. (24) and (32) are independent. We then have a total of $2(N_\beta - 1)(N_\gamma - 1)$ independent equations from compatibility.

4.3.3. Matrix form of the equations

Altogether, there are $2(N_\beta + N_\gamma) + N_\beta N_\gamma + 1$ equations from the average strain relationships, $3(N_\beta N_\gamma - 1)$ equations from equilibrium, and $2(N_\beta - 1)(N_\gamma - 1)$ equations from compatibility. This gives a total of $6N_\beta N_\gamma$ equations for $6N_\beta N_\gamma$ unknown subcell strains. These equations can be written in matrix form as:

$$\tilde{\mathbf{A}} \boldsymbol{\varepsilon}_s = \tilde{\mathbf{K}} \bar{\boldsymbol{\varepsilon}} \tag{38}$$

where

$$\tilde{\mathbf{A}} \equiv \begin{bmatrix} \tilde{\mathbf{A}}_G \\ \tilde{\mathbf{A}}_M \\ \tilde{\mathbf{A}}_C \end{bmatrix} \tag{39}$$

and,

$$\tilde{\mathbf{K}} \equiv \begin{bmatrix} \tilde{\mathbf{J}} \\ \mathbf{0} \\ \mathbf{0} \end{bmatrix} \tag{40}$$

where the submatrices $\tilde{\mathbf{A}}_G$, $\tilde{\mathbf{A}}_M$, and $\tilde{\mathbf{J}}$ are analogous to those in Eqs. (18)–(19), and $\tilde{\mathbf{A}}_C$ is a new matrix that results from the compatibility relationships.

5. Determination of effective elastic constants

GMC and SCMC require the solution of the linear systems (17) and (38). These solutions result in so called strain concentration factors (Hill, 1964). The following steps illustrate the procedure to find these concentration factors for SCMC. The procedure for GMC is completely analogous.

First, Eq. (38) is premultiplied by $\tilde{\mathbf{A}}^{-1}$ to yield:

$$\boldsymbol{\varepsilon}_s = \tilde{\mathbf{A}}_s \bar{\boldsymbol{\varepsilon}} \tag{41}$$

where $\tilde{\mathbf{A}}_s \equiv \tilde{\mathbf{A}}^{-1}\tilde{\mathbf{K}}$ is a matrix of concentration factors. This matrix is now partitioned into $N_\beta N_\gamma$ 6×6 submatrices, each relating the effective strains to the strains in a specific subcell. Let each of these 6×6 concentration factor submatrices be denoted $\tilde{\mathbf{A}}_s^{(\beta\gamma)}$. Then, an expression analogous to Eq. (41) can be written for each subcell as:

$$\boldsymbol{\varepsilon}^{(\beta\gamma)} = \tilde{\mathbf{A}}_s^{(\beta\gamma)} \bar{\boldsymbol{\varepsilon}} \tag{42}$$

Premultiplication of Eq. (42) by $\mathbf{C}^{(\beta\gamma)}$ yields:

$$\boldsymbol{\sigma}^{(\beta\gamma)} = \mathbf{C}^{(\beta\gamma)} \tilde{\mathbf{A}}_s^{(\beta\gamma)} \bar{\boldsymbol{\varepsilon}}, \tag{43}$$

and application of a definition of average stresses analogous to Eq. (7), results in:

$$\bar{\boldsymbol{\sigma}} \equiv \frac{1}{hl} \sum_{\beta}^{N_\beta} \sum_{\gamma}^{N_\gamma} h_\beta l_\gamma \mathbf{C}^{(\beta\gamma)} \tilde{\mathbf{A}}_s^{(\beta\gamma)} \bar{\boldsymbol{\varepsilon}} \tag{44}$$

which suggests the following definition for the effective (average) stiffness matrix:

$$\bar{\mathbf{C}} \equiv \frac{1}{hl} \sum_{\beta}^{N_\beta} \sum_{\gamma}^{N_\gamma} h_\beta l_\gamma \mathbf{C}^{(\beta\gamma)} \tilde{\mathbf{A}}_s^{(\beta\gamma)} \tag{45}$$

6. Micromechanical analysis using the FEM

The FEM results reported in the present study were obtained using an in-house 3D finite element code. The RVE was discretized with displacement-based 8-noded linear elements (see Fig. 3). The average strain relationships are enforced in the FEM model by requiring that the displacements at the interfaces of the (in this case) 3D unit cell be linked in such a way that the strains satisfy 3D versions of Eqs. (1)–(6). Referring for instance to nodes i and k in Fig. 3, the displacements $\mathbf{u}_k$ and $\mathbf{u}_i$ are related by:

$$\mathbf{u}_k = \mathbf{u}_i + \mathbf{E}(\mathbf{r}_k - \mathbf{r}_i) \tag{46}$$

where $\mathbf{r}_i$ and $\mathbf{r}_k$ are the position vectors of points i and k, respectively; and $\mathbf{E}$ is the effective strain tensor as previously defined.

It should be pointed out that even though SCMC and the FEM are clearly distinct methods, they satisfy asymptotically the same elasticity equations. The displacement-based FEM is a general method to solve boundary value problems that uses displacements as unknowns. In contrast, SCMC is a specific method that is entirely formulated in terms of stresses and strains. Furthermore, the main

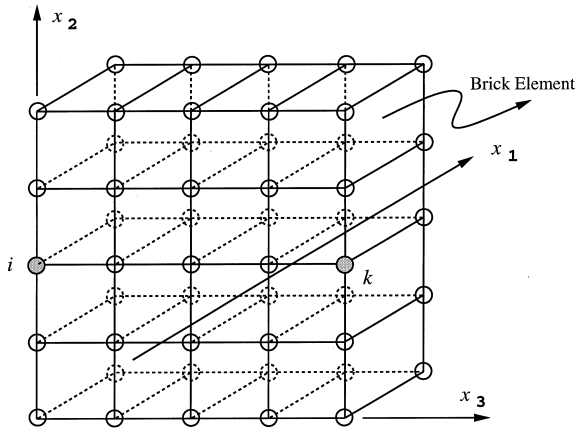

Fig. 3. Sample FEM discretization of unit cell using 8-noded 3D elements.

matrices of these two methods have a different number of nonzero entries as it will be shown in the next section. In the FEM, equilibrium is approximate and satisfied exactly only as the mesh is refined. Also, the constitutive equations are incorporated exactly into the finite element model, and compatibility is automatically satisfied since the displacement field is single valued. In the SCMC approach, the constitutive equations are also incorporated exactly into the model, and compatibility and equilibrium are approximated by finite differences. As a result, the difference between results obtained with SCMC and the FEM must come mainly from the approximation of the compatibility equations. As it will be observed in the next section, this difference is small and tends to zero as the discretization is refined.

7. Numerical results

In order to assess the accuracy and computational efficiency of SCMC, three kinds of numerical experiments were performed. The first one consisted of computing the subcell stresses for a given effective stress. This was carried out for the three methods, e.g., SCMC, GMC, and the FEM. Two types of microstructures were considered, a microstructure with a random distribution of fiber material (Fig. 4), and a microstructure with a single square fiber (Fig. 5). In all numerical experiments the composite microstructures consisted of isotropic boron fibers embedded in an aluminum matrix. The elastic constants are presented in Table 1.

The second type of numerical experiment consisted of comparing the effective elastic constants obtained with SCMC, GMC, the FEM, the Reuss, and the Voigt approximations. This was

Table 1
Material properties of Boron/Aluminum composite used in the numerical experiments (from Ref. Budiansky, 1965)

Material	E (GPa)	ν
Boron	413.7	0.2
Aluminum	55.16	0.3

performed for a microstructure with a hexagonal packing of fiber material and a varying fiber volume fraction.

Finally, the third numerical experiment consisted of a comparison of the effective elastic constants of the random microstructure and the single square fiber microstructure as a function of the number of subdomains.

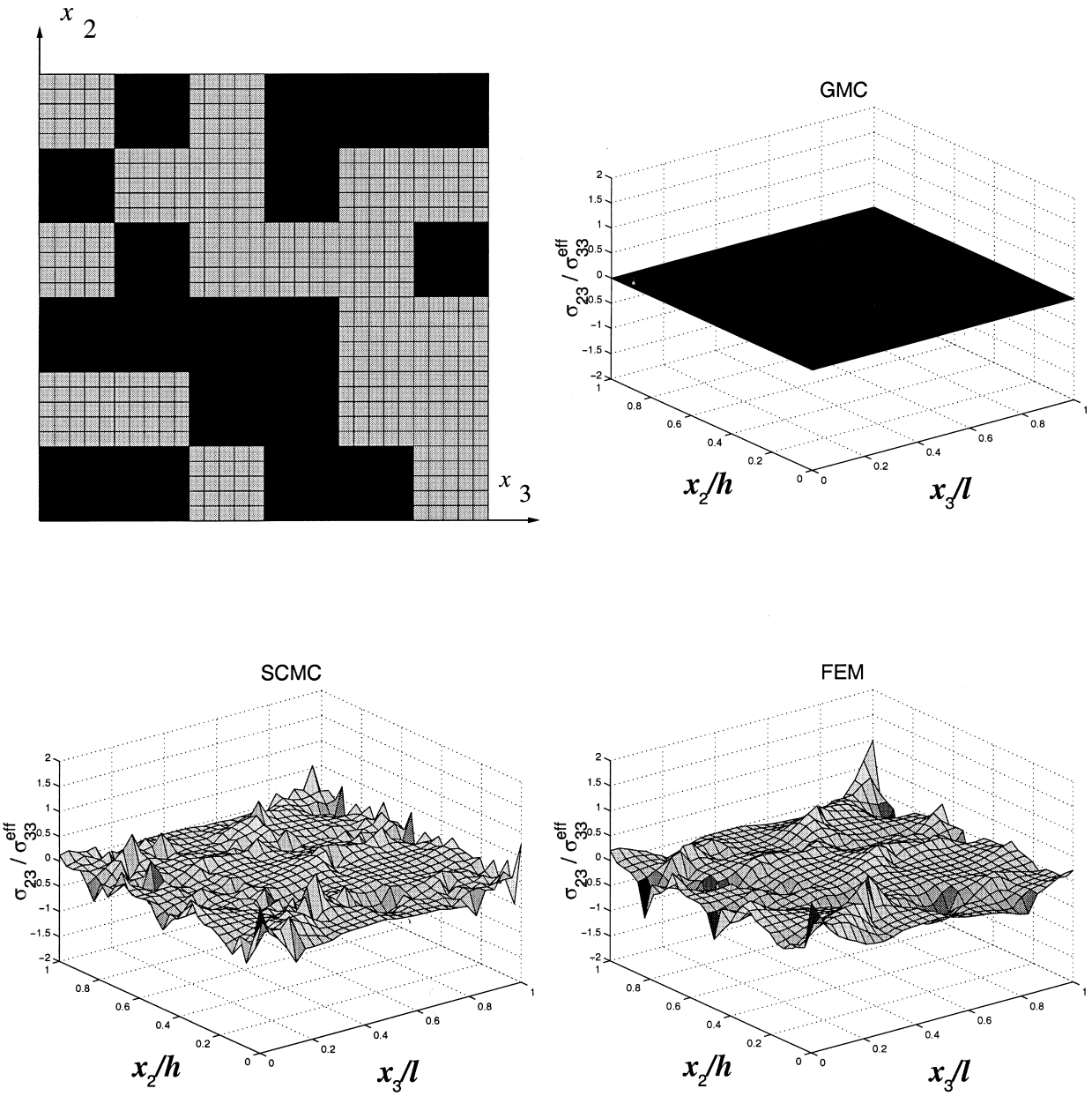

Fig. 4. $\sigma_{23}/\bar{\sigma}_{33}$ for a composite with random fiber inclusions. $V_f = 0.5$, $N_\beta = N_\gamma = 30$.

7.1. Prediction of subcell stresses

As mentioned, one of the most important features of SCMC is its capability to model coupling between normal and shear components of stress. This shear coupling feature is illustrated in Fig. 4 for the normalized stresses $\sigma_{23}/\bar{\sigma}_{33}$ of a random microstructure, and in Fig. 5 for the normalized stresses $\sigma_{23}/\bar{\sigma}_{22}$ in a composite with uniformly distributed square fibers. It can be seen that, in these cases, GMC

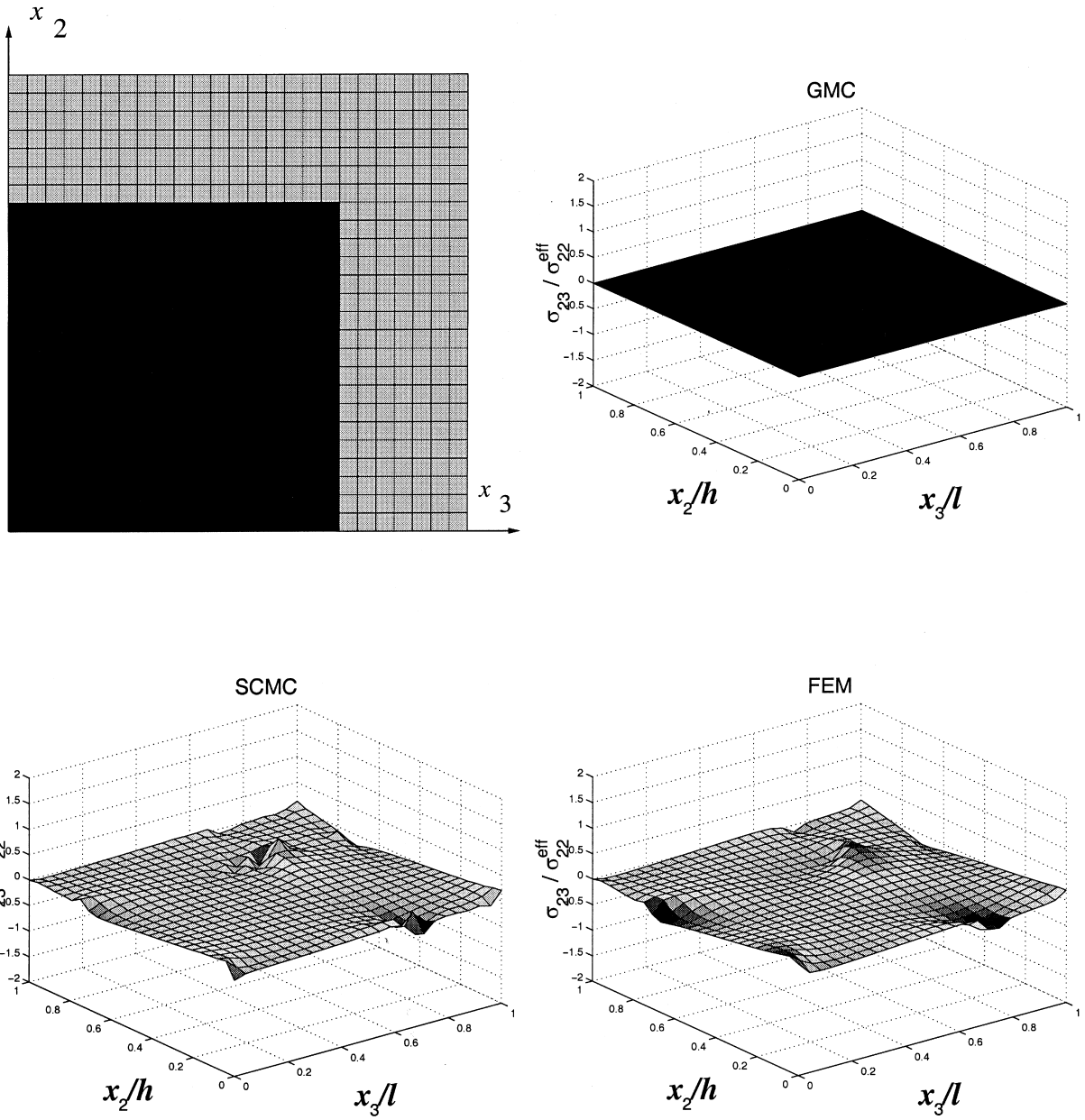

Fig. 5. $\sigma_{23}/\bar{\sigma}_{22}$ for a composite with square fibers. $V_f = 0.5$, $N_\beta = N_\gamma = 25$.

predicts zero shear stresses while SCMC and the FEM predict nonzero subcell shear stresses. It can be shown that the average shear stress for the SCMC and FEM results is zero as it should be. It can also be observed from the figures that the peak transverse shear stresses are higher for the random microstructure as could be expected. Finally, it is observed that the SCMC and FEM results are very similar in all cases.

Numerical experiments for subcell stresses were performed for all the six components of the effective stress. A summary of qualitative results for all cases studied is presented in Table 2. Quantitative results are presented for a few noteworthy cases in Figs. 6–10. Fig. 6 illustrates the distribution of $\sigma_{11}/\bar{\sigma}_{11}$ within the unit cell, for a nonzero $\bar{\sigma}_{11}$. It can be observed that, in this case, all the three methods yield exactly the same result.

Table 2
Summary of results for subcell stresses experiment

Loading ($\bar{\sigma}_*$)	Subcell stress (σ_*)	Normalized stress ($\sigma_*/\bar{\sigma}_*$)			Comments
		SCMC	FEM	GMC	
$\bar{\sigma}_{11}$	σ_{11}	nonzero	nonzero	nonzero	All methods same values (Fig. 6)
	σ_{22}	nonzero	nonzero	nonzero	Different numerical values
	σ_{33}	nonzero	nonzero	nonzero	Different numerical values
	σ_{23}	nonzero	nonzero	zero	
	σ_{13}	zero	zero	zero	
	σ_{12}	zero	zero	zero	
$\bar{\sigma}_{22}$	σ_{11}	nonzero	nonzero	nonzero	Different numerical values
	σ_{22}	nonzero	nonzero	nonzero	See Fig. 9
	σ_{33}	nonzero	nonzero	nonzero	Different numerical values
	σ_{23}	nonzero	nonzero	zero	Shear coupling (See Fig. 5)
	σ_{13}	zero	zero	zero	
	σ_{12}	zero	zero	zero	
$\bar{\sigma}_{33}$	σ_{13}	nonzero	nonzero	nonzero	Different numerical values
	σ_{22}	nonzero	nonzero	nonzero	Different numerical values
	σ_{33}	nonzero	nonzero	nonzero	Different numerical values
	σ_{23}	nonzero	nonzero	zero	Shear coupling (See Fig. 4)
	σ_{13}	zero	zero	zero	
	σ_{12}	zero	zero	zero	
$\bar{\sigma}_{23}$	σ_{11}	nonzero	nonzero	zero	
	σ_{22}	nonzero	nonzero	zero	Shear coupling (See Fig. 8)
	σ_{33}	nonzero	nonzero	zero	
	σ_{23}	nonzero	nonzero	1.0	See Fig. 7
	σ_{13}	zero	zero	zero	
	σ_{12}	zero	zero	zero	
$\bar{\sigma}_{13}$	σ_{11}	zero	zero	zero	
	σ_{22}	zero	zero	zero	
	σ_{33}	zero	zero	zero	
	σ_{23}	zero	zero	zero	
	σ_{13}	nonzero	nonzero	nonzero	See Fig. 10
	σ_{12}	nonzero	nonzero	zero	Shear coupling
$\bar{\sigma}_{12}$	σ_{11}	zero	zero	zero	
	σ_{22}	zero	zero	zero	
	σ_{33}	zero	zero	zero	
	σ_{23}	zero	zero	zero	
	σ_{13}	nonzero	nonzero	zero	Shear coupling
	σ_{12}	nonzero	nonzero	nonzero	

Fig. 7 illustrates the distribution of the transverse shear stress due to a nonzero effective shear stress (the "self-response" of the shear stress). It can be seen that while GMC predicts a uniform subcell shear stress (equal to the applied effective stress), SCMC and the FEM predict non-uniform subcell shear stresses.

Shear coupling is also illustrated in Fig. 8. In this case, the distribution of the normal stresses is plotted for a given nonzero applied effective stress $\bar{\sigma}_{23}$.

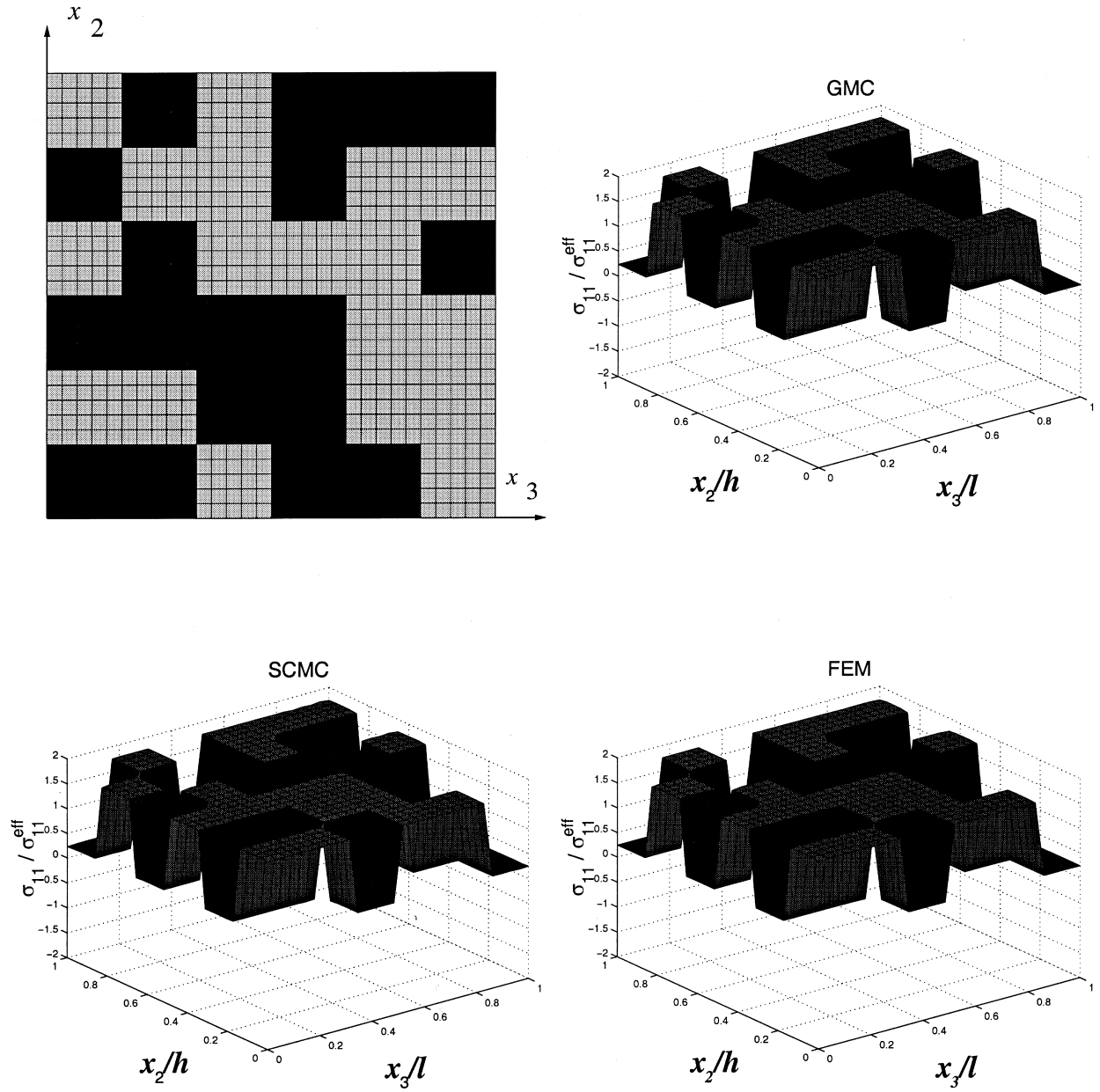

Fig. 6. $\sigma_{11}/\bar{\sigma}_{11}$ for a composite with random fiber Inclusions. $V_f = 0.5$, $N_\beta = N_\gamma = 30$.

There is also coupling between σ_{13} and σ_{12}. It is observed that in this case GMC predicts no coupling while SCMC and the FEM predict non-uniform, nonzero subcell stresses (See Table 2).

Finally, Figs. 9 and 10 illustrate the "self-responses" of σ_{22} and σ_{13}. Fig. 9 illustrates the fact that GMC predicts no variation of σ_{22} along the x_2 direction. Conversely, Fig. 10 illustrates the fact that GMC predicts no variation of σ_{13} along the x_3 direction. These results are a direct consequence of the traction continuity conditions. A similar phenomenon is observed for the self-responses of σ_{12} and σ_{33} (not shown).

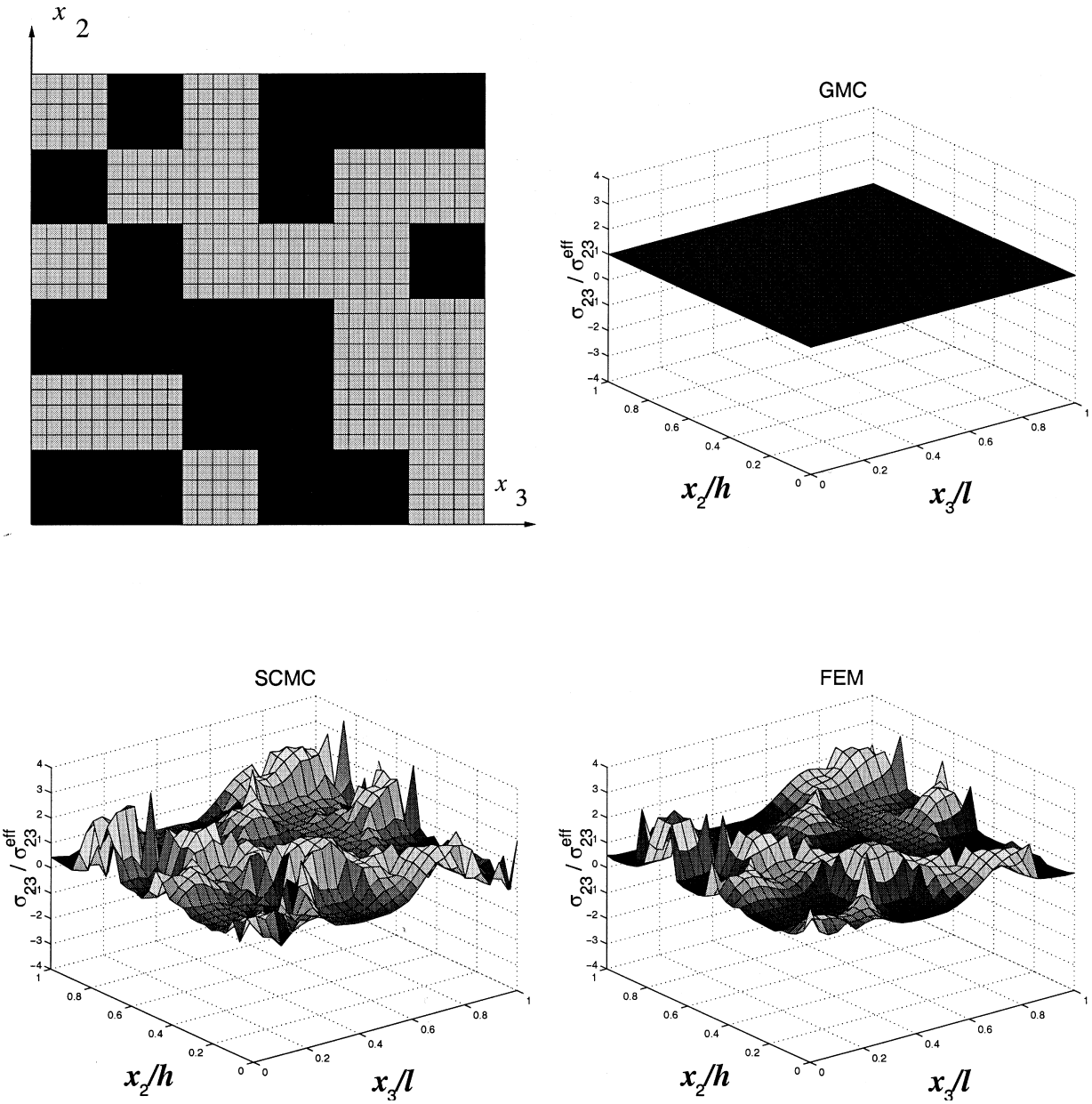

Fig. 7. $\sigma_{23}/\bar{\sigma}_{23}$ for a composite with random fiber inclusions. $V_f = 0.5$, $N_\beta = N_\gamma = 30$.

7.2. Prediction of elastic constants

The fact that GMC is capable of modelling, with sufficient accuracy, the mechanical response and the elastic constants of multi-phase composites over a wide range of conditions and behavior is well established (see e.g., Lissenden and Herakovich, 1992; Aboudi, 1991; Orozco, 1997). Due to GMC's

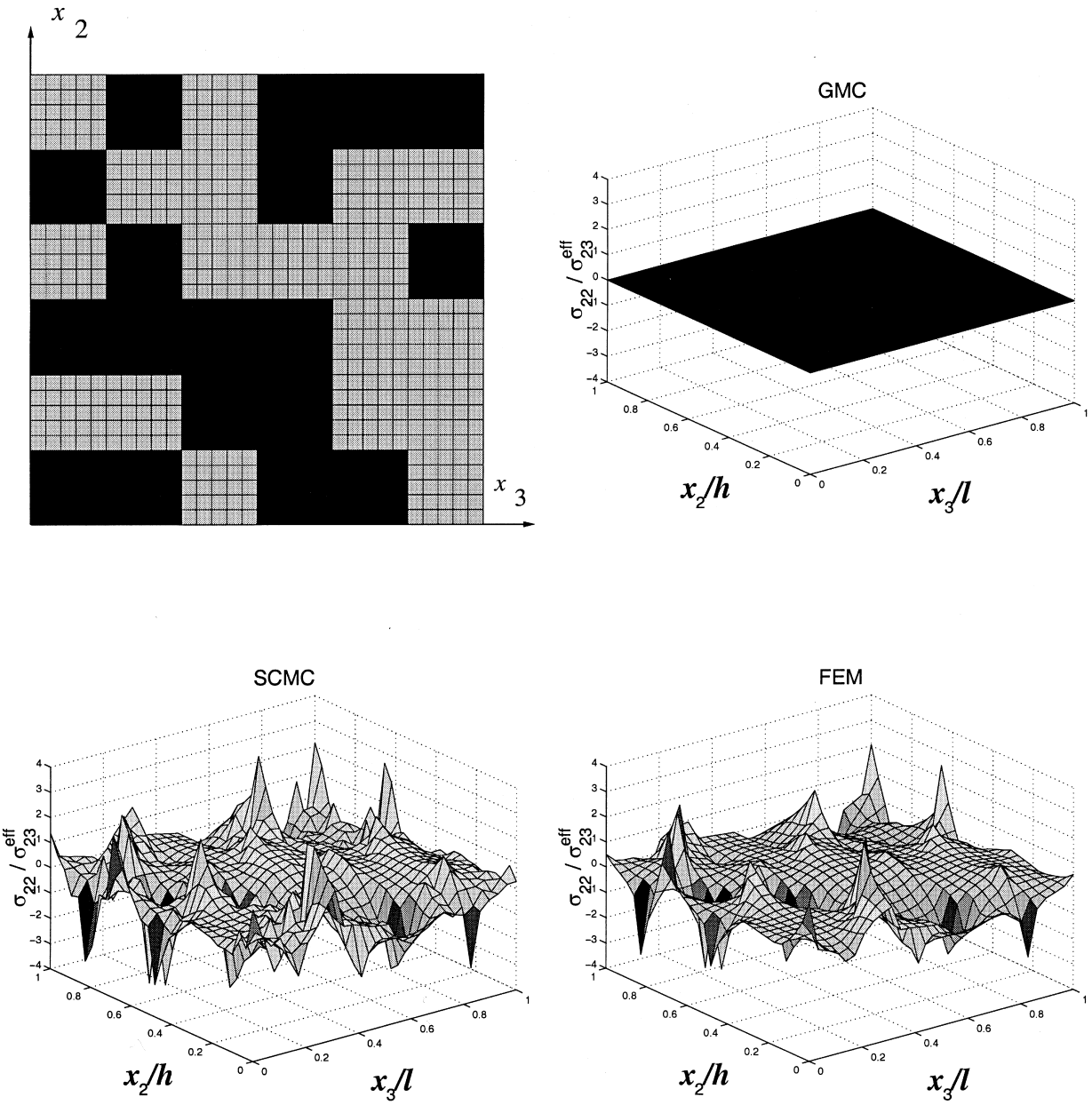

Fig. 8. $\sigma_{22}/\bar{\sigma}_{23}$ for a composite with random fiber inclusions. $V_f = 0.5$, $N_\beta = N_\gamma = 30$.

traction continuity assumption however, *monoclinic* behavior is approximated with *orthotropic* behavior. The responses shown in Figs. 9 and 10 constitute an example of this. This of course has an adverse effect on the estimation of the effective elastic constants of the composite, especially when the material is monoclinic. Since SCMC and the FEM are free from the traction continuity condition, they can model monoclinic materials quite accurately. In this section, we compare elastic constant predictions by SCMC, GMC, the FEM, the Reuss and the Voigt approximations for the hexagonal microstructure

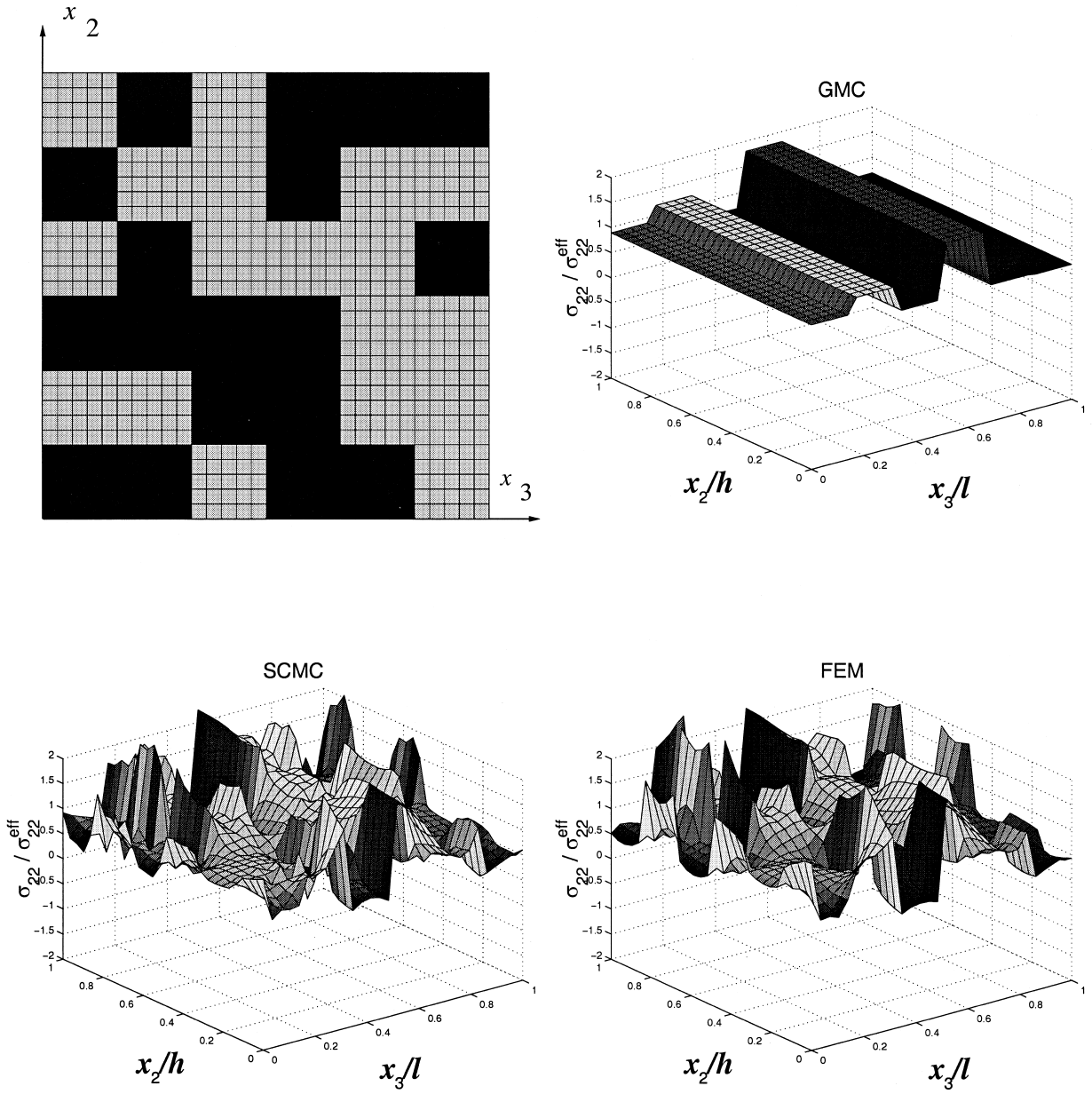

Fig. 9. $\sigma_{22}/\bar{\sigma}_{22}$ for a composite with random fiber inclusions. $V_f = 0.5$, $N_\beta = N_\gamma = 30$.

shown in Fig. 11. We also compare GMC, SCMC, and the FEM for the random and the square fiber microstructures of the previous section.

7.2.1. Elastic constants as a function fiber volume fraction

The comparison between SCMC, GMC, the FEM, the Reuss, and the Voigt approximations was first

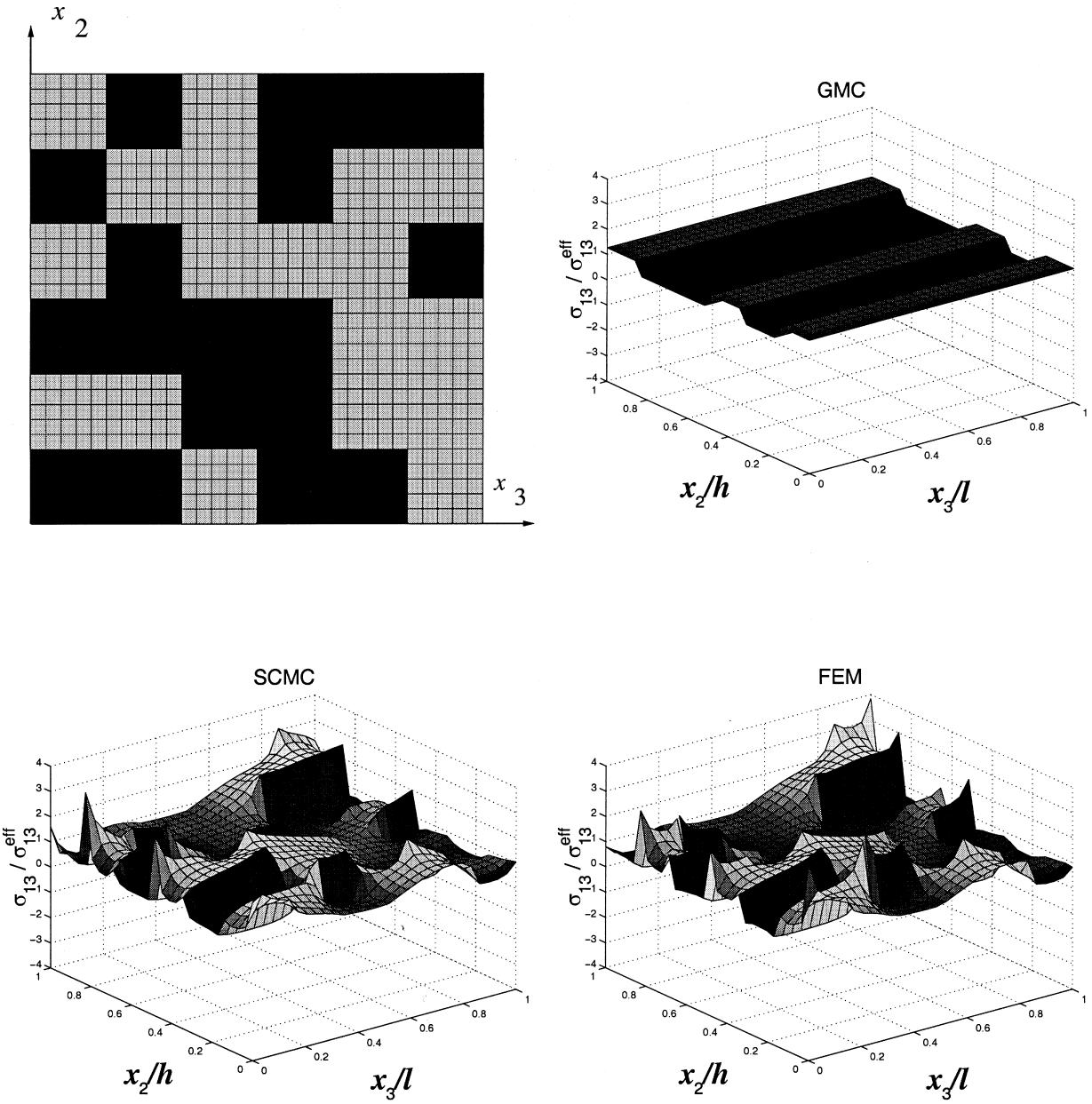

Fig. 10. $\sigma_{13}/\bar{\sigma}_{13}$ for a composite with random fiber Inclusions. $V_f = 0.5$, $N_\beta = N_\gamma = 30$.

made for a varying fiber volume fraction in the composite. A hexagonal microstructure (Fig. 11) was used in this experiment. This particular microstructure was chosen because its properties closely approximate those of a transversely isotropic material. This allows for a fair comparison of GMC, SCMC, and the FEM with the Voigt and Reuss models which rely on relative volume fractions of the phases only (see e.g., Herakovich, 1998). Results for six elastic constants are presented in Figs. 11 and 12. It can be seen that all methods produce identical estimates for E_{11} except the Reuss model (Fig. 11). This is because of Reuss' fundamental assumption that the local stresses are equal to the effective stress.

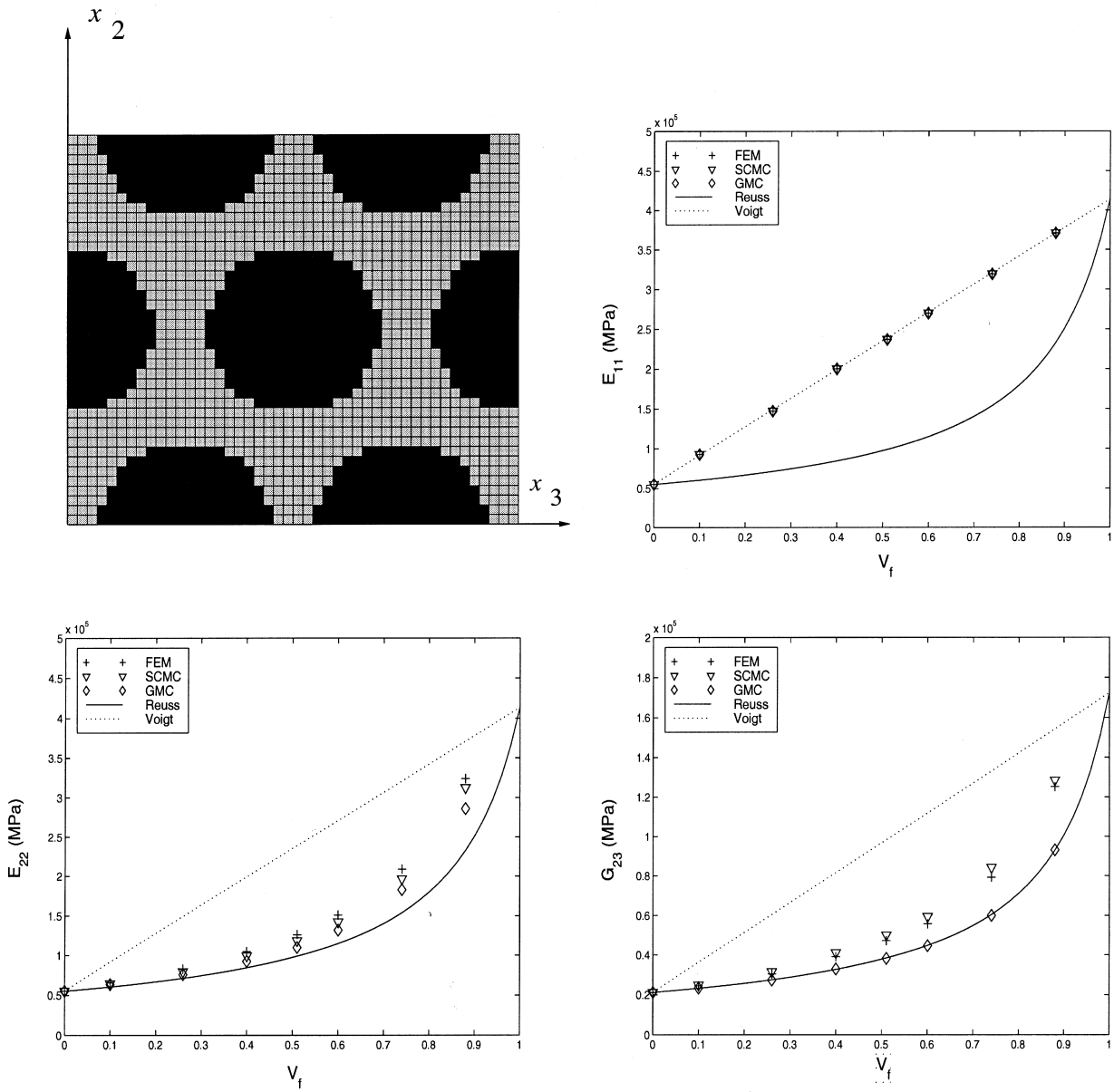

Fig. 11. Elastic constants. Unit cell with hexagonal packing. $V_f = 0.5$, $N_\beta = 46, N_\gamma = 40$.

It can also be observed that for E_{22}, SCMC, and the FEM produce very similar estimates. On the other hand, GMC's approximation of G_{23} is identical to that of the Reuss approximation. In all the cases shown in Fig. 12, it is observed that SCMC and the FEM produce very similar estimates. In general, GMC estimates are also very similar to those of the FEM and SCMC, except for G_{23}, G_{12} and G_{13} (not shown).

In summary, it was found that GMC, SCMC, and the FEM produce elastic constant estimates that are very similar to each other. Due to the lack of shear coupling however, GMC estimates for G_{23}, G_{12}

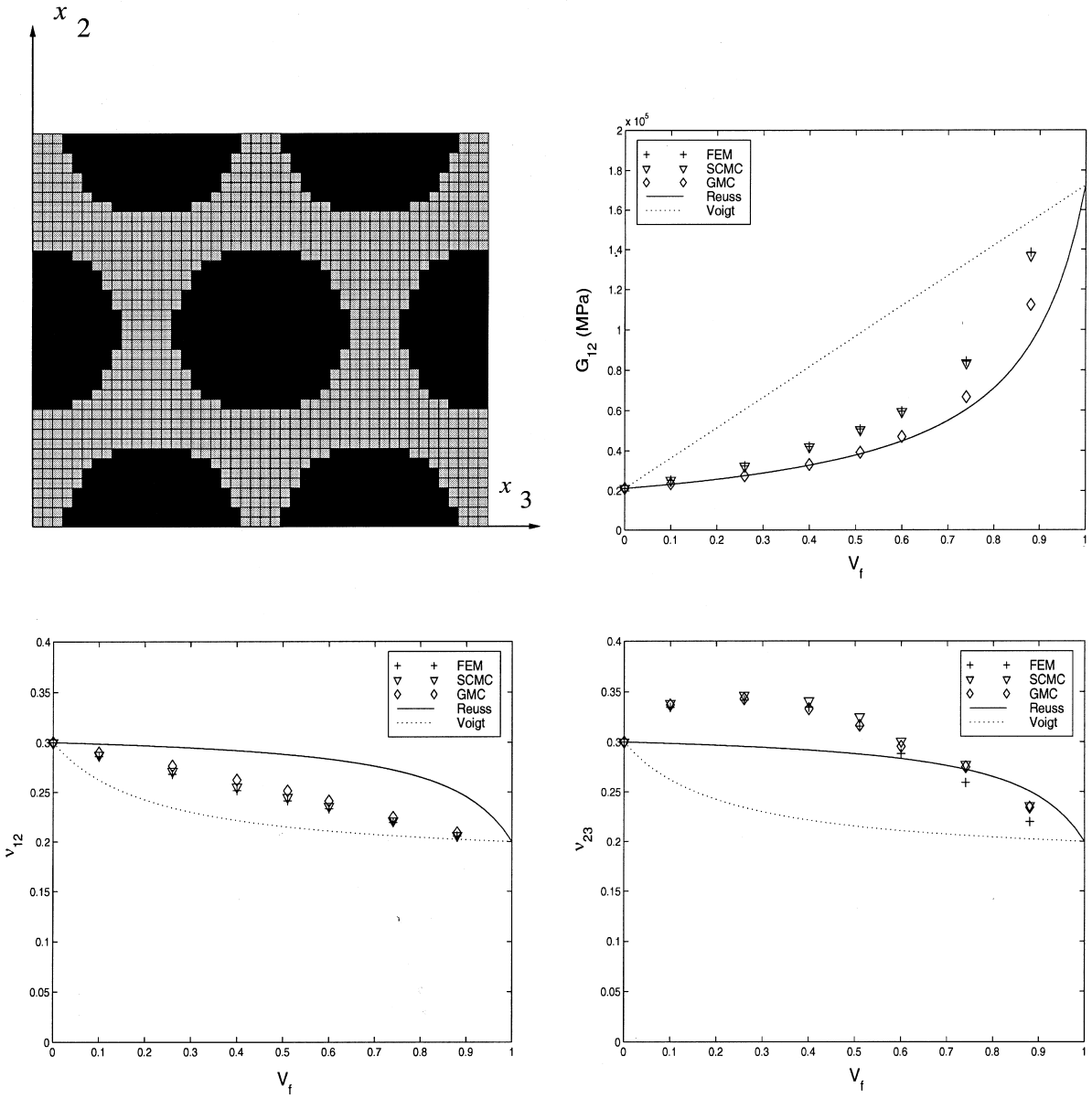

Fig. 12. Elastic constants. Unit cell with hexagonal packing. $V_f = 0.5$. $N_\beta = 46, N_\gamma = 40$.

and G_{13} tend to be far from those of the other two methods. GMC estimates of the shear moduli are in fact very close to the lower bound represented by the Reuss approximation.

7.2.2. Elastic constants as a function of the number of subdomains

In this numerical experiment, the number of subdomains in the RVE (subcells for SCMC and GMC and finite elements for the FEM) was sequentially increased. For the random microstructure, the sequence was: 6×6, 12×12, 18×18, 24×24 and 30×30. For the microstructure with the square fiber,

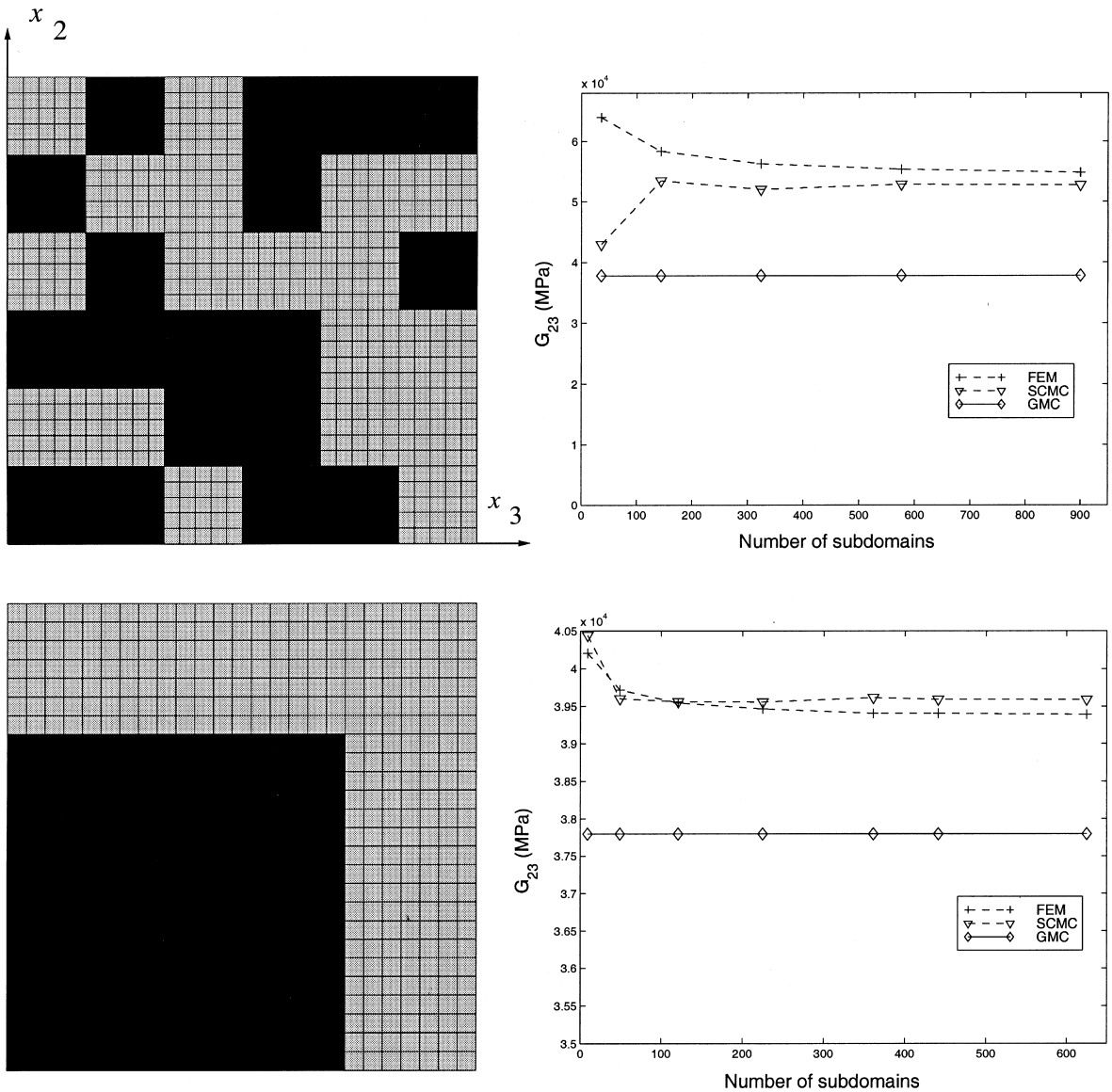

Fig. 13. Elastic constants for random and square arrays of a Boron/Aluminium composite. $V_f = 0.5$. Top left: $N_\beta = N_\gamma = 30$. Bottom left: $N_\beta = N_\gamma = 25$.

Table 3
Comparison of elastic constants for composite with square fiber (25 × 25) — Percent difference relative to FEM results. Elastic moduli in GPa

Constant	FEM	GMC	% difference	SCMC	% difference
E_{11}	234.7	234.7	0.00	234.7	0.00
E_{22}	137.4	130.8	−4.80	135.6	−1.31
E_{33}	137.4	130.8	−4.80	135.6	−1.31
ν_{12}	0.2428	0.2446	0.74	0.2433	0.20
ν_{13}	0.2428	0.2446	0.74	0.2433	0.20
ν_{23}	0.2396	0.2568	7.17	0.2440	1.83
G_{23}	39.39	37.79	−4.06	39.59	−0.50
G_{13}	49.35	45.73	−7.33	49.28	−0.14
G_{12}	49.35	45.73	−7.33	49.28	−0.14

the sequence was 7 × 7, 15 × 15, 20 × 20 and 25 × 25. These sequences guarantee an increase in the number of subdomains while keeping the fiber volume fraction approximately constant (at about 0.5). Fig. 13 illustrates the results obtained in this manner for the transverse shear modulus. The first observation from Fig. 13 is that the GMC approximation does not vary with the number of subdomains. In other words, GMC results are *mesh independent*. This is actually an advantage of GMC over SCMC and the FEM since it means that estimates of the properties and behavior of the composite can be obtained at a relatively low cost. By the same token, it can be seen that the SCMC and the FEM approximations do not change much after about 200 subdomains (See Fig. 13). These two methods are nevertheless *mesh dependent* and the approximations improve in general, by refining the discretization. In Fig. 13, it can be seen that the maximum difference between estimates occurs between GMC and the FEM for the random microstructure. This difference is of the order of 17%. Other results for elastic constant estimates are summarized in Tables 3 and 4. These correspond to discretizations using the maximum number of subdomains (900). The error in Tables 3 and 4 is given with respect to the FEM estimate. It can be seen that the maximum errors occur for the GMC estimates of G_{12}, G_{13} and G_{23}. They are of the order of 7% for the microstructure with the square fiber and of the order of 30% for the random microstructure.

Table 4
Comparison of elastic constants for composite with a random microstructure (30 × 30) — Percent difference relative to FEM results. Elastic moduli in GPa

Constant	FEM	GMC	% difference	SCMC	% difference
E_{11}	234.7	234.7	0.00	234.7	0.00
E_{22}	138.5	117.9	−14.8	131.0	−5.41
E_{33}	137.3	113.1	−17.6	128.6	−6.36
ν_{12}	0.2361	0.2446	3.60	0.2387	1.10
ν_{13}	0.2369	0.2492	5.19	0.2405	1.51
ν_{23}	0.3078	0.3289	6.85	0.3182	3.37
G_{23}	54.78	37.78	−31.0	57.70	5.33
G_{13}	60.99	40.53	−33.5	58.77	−3.63
G_{12}	60.48	42.94	−29.0	58.51	−3.25

Table 5
Performance comparison between GMC, SCMC, and FEM — Small problem

Method	Subcell arrangement	No. of subcells	Nonzeros in **A**	CPU (s) (SUN Sparc-20)	Speed-up wrt. FEM
GMC	6×6	36	766	0.23	298
SCMC	12×12	144	4074	2.39	29
FEM	12×12	144	6102	68.6	1

8. Computational issues

SCMC matrices, just as GMC's and FEM's have a large number of zero entries. As a result, sparse implementations of these methods are most advantageous (Orozco, 1997). All numerical results reported here were obtained using sparse implementations of GMC, SCMC, and the FEM. The sparse factorization package available in the IMSL mathematical library was used to solve the linear systems. A comparison of the computational efficiency of the three methods is presented below. The comparison is presented for a small problem and for a moderate size problem. The small problem comparison is shown in Table 5 and corresponds to a 6×6 unit cell for GMC, and a 12×12 unit cell for SCMC and the FEM. This particular choice was made because 12×12 is the smallest discretization for which SCMC and the FEM achieve a "good enough" value of the elastic constant estimates. Since GMC is mesh independent, results were obtained for a 6×6 discretization (see Fig. 13).

For the small problem (Table 5), GMC is about 300 hundred times more efficient than the FEM, while SCMC is 30 times more efficient than the FEM. The comparison for the moderate size problem is presented in Table 6. This corresponds to a 30×30 unit cell for all the three methods. In this case, GMC is 42 times faster than the FEM, while SCMC is six times faster. The number of nonzero entries in the main matrices of the different methods is also shown in Tables 5 and 6. It can be seen that the number of nonzero entries is directly related to the CPU times reported as it might be expected.

9. Concluding remarks

A new volume-averaging method for micromechanical analysis of multi phase composites called Strain-Compatible Method of Cells (SCMC) has been presented. The method is inspired by the well known generalized method of cells (GMC). In contrast to GMC, however, SCMC exhibits the so called "shear coupling" between the normal and shear stresses. In the present study, the new method has been used to model the elastic constants and the micro-stresses of unidirectional composites. SCMC's accuracy and performance have been compared with those of GMC and those of the finite element method. It has been found that SCMC results are consistent with the results of the finite element

Table 6
Performance comparison between GMC, SCMC and FEM — Moderate size problem

Method	Subcell arrangement	No. of subcells	Nonzeros in **A**	CPU (s) (RS 6000)	Speed-up wrt. FEM
GMC	30×30	900	17,638	12.4	42
SCMC	30×30	900	35,154	87.8	6
FEM	30×30	900	41,166	523.6	1

method. In addition, the resulting SCMC matrix equations are formally equivalent to those of GMC, which results in an efficient numerical implementation. In particular, either SCMC or GMC formulations are more convenient than those of the traditional FEM because they completely eliminate the need to model boundary conditions. Furthermore, both SCMC and GMC provide three-dimensional characterizations of the composite with just a two-dimensional model (unit cell). In order to obtain the same information using the FEM, it is usually necessary to resort to three-dimensional elements. As far as computational performance is concerned, the computational cost of SCMC is higher than that of GMC but about 1/6th of that of the traditional FEM. The new method can be readily extended to deal with three-dimensional composite microstructures and with nonlinear behavior.

Acknowledgements

The authors are grateful to Professor Jacob Aboudi of Tel-Aviv University for many useful discussions and suggestions. The authors are also grateful to the reviewers of the manuscript for the thoroughness of their work and their comments and suggestions.

References

Aboudi, J., 1991. Mechanics of Composite Materials — A Unified Micromechanical Approach. Elsevier, Amsterdam, New York.

Aboudi, J., 1996. Micromechanical analysis of composites by the method of cells-update. Applied Mech. Rev 49 (10), S83–S91.

Benveniste, Y., 1987. A new approach to the application of the Mori–Tanaka theory in composite materials. Mechanics of Materials 36, 147–157.

Budiansky, B., 1965. On the elastic moduli of some heterogeneous materials. Mechanics and Physics of Solids 13, 223–227.

Hashin, Z., Rosen, B.W., 1964. The elastic moduli of fiber-reinforced materials. Journal of Applied Mechanics 31, 223–232.

Herakovich, C.T., 1998. Mechanics of Fibrous Composites. Wiley, New York.

Hill, R., 1964. Theory of mechanical properties of fibre-strengthened materials. Part I: Elastic behavior. Mechanics and Physics of Solids 12, 199–212.

Hill, R., 1965. A self-consistent mechanics of composite materials. Mechanics and Physics of Solids 13 (4), 213–222.

Lissenden, C.J., Herakovich, C.T., 1992. Comparison of micromechanical models for elastic properties. In: Sadeh, W.Z., Sture, S., Miller, R.J. (Eds.), Space '92, Proc. 3rd Int. Conference, Engineering, Construction and Operations in SPACE III. ASCE, New York, pp. 1309–1322.

Mori, T., Tanaka, K., 1973. Average stress in matrix and average elastic energy of materials with misfitting inclusions. Acta Metall 21, 571–574.

Orozco, C.E., 1997. Computational aspects of modelling complex microstructure composites using GMC. Composites Engineering 28B, 167–175.

Ostoja-Starzewski, M., 1998. Random field models of heterogeneous materials. International Journal of Solids and Structures 35 (19), 2429–2455.

Paley, M., Aboudi, J., 1992. Micromechanical analysis of composites by the generalized method of cells. Mechanics of Materials 14, 127–139.

Reuss, A., 1929. Berechnung der Fliessgrenze von Mischkristallen auf Grund der Plastizitätsbedingung für Einkristalle. Z. Angew. Math. Mech 9, 49–58.

Voigt, W., 1889. Über die Beziehungen zwischen den beiden Elastizitäskonstanten isotroper Körper. Wied. Ann 38, 573–587.